Neuron, Vol. 16, 983–990, May, 1996, Copyright ©1996 by Cell Press

Subunit Stoichiometry of Cyclic Nucleotide-Gated Channels and Effects of Subunit Order on Channel Function

David T. Liu,* Gareth R. Tibbs,† and Steven A. Siegelbaum†‡§
*Integrated Program in Cellular, Molecular, and Biophysical Studies
†Center for Neurobiology and Behavior
‡Department of Pharmacology
§Howard Hughes Medical Institute
Columbia University
New York, New York 10032

Summary

Cyclic nucleotide-gated (CNG) ion channels are multimeric structures containing at least two subunits. However, the total number of subunits per functional channel is unknown. To determine the subunit stoichiometry of CNG ion channels, we have coexpressed the 30 pS conductance bovine retinal channel (RET) with an 85 pS conductance chimeric retinal channel containing the catfish olfactory channel P region (RO133). When RO133 and RET monomers are coexpressed, channels with four distinct intermediate conductances are observed. Dimer constructs reveal that two of these conductance levels arise from channels with the same subunit composition (2 RO133:2 RET) but distinct subunit order (like subunits adjacent to each other versus like subunits across from each other). Thus, the data demonstrate that cyclic nucleotide-gated ion channels are tetrameric like the related voltage-gated potassium ion channels; the order of subunits affects the conductance of the channel; and the channel has 4-fold symmetry in which four asymmetric subunits assemble head to tail around a central axis.

Introduction

Both voltage-gated and ligand-gated ion channels are multimeric proteins with distinct subunit stoichiometry. Ligand-gated channels related to the nicotinic ACh receptors are thought to be composed of five pore-forming subunits (Karlin, 1993; Cooper et al., 1991). Voltage-gated channels are composed of either four pore-forming subunits, in the case of K channels (MacKinnon, 1991; Liman et al., 1992), or a single pore-forming subunit with four internal repeats that serve as pseudosubunits, in the case of Na (Catterall, 1992) and Ca channels (Hofmann et al., 1994). In addition to their major pore-forming subunits, voltage-gated channels are often associated with smaller subunits that modulate the function of the channel (Isom et al., 1994).

Ligand-gated channels and voltage-gated K channels are thought to exist as heteromultimers composed of more than one type of pore-forming subunit (Karlin, 1993; Isacoff et al., 1990; Ruppersberg et al., 1990; Christie et al., 1990). These heteromultimers often exhibit properties that are distinct from the homomultimeric channels formed by each component subunit (Mishina et al., 1990; Isacoff et al., 1990; Ruppersberg et al., 1990; Christie et al., 1990). Thus, the formation of heteromultimers can increase the diversity of functional channel types obtainable with a limited number of subunit genes, allowing neurons to fine-tune their electrophysiological properties. Further diversity is theoretically possible if channels with identical subunit composition but different subunit order around the central axis of the pore have distinct properties. However, to date, there is little direct evidence to suggest that subunit order influences physiological function of ion channels.

The cyclic nucleotide-gated (CNG) ion channels form an interesting link between the ligand-gated and voltage-gated channel families. The CNG channels, which play important roles in visual and olfactory signal transduction (Yau and Baylor, 1989; Nakamura and Gold, 1987; Zagotta and Siegelbaum, 1996), are activated by the binding of intracellular cyclic nucleotides, and thus function as ligand-gated channels. However, the primary amino acid sequence of CNG channels is similar to that of voltage-gated K channels (Jan and Jan, 1990; Goulding et al., 1992), indicating that they are members of the voltage-gated channel superfamily. Like the K channels, CNG channel subunits are thought to contain six transmembrane domains, including an S4 region that is homologous to the S4 voltage- sensor of voltage-gated channels. The CNG channels also contain a pore-lining P region linking the S5 and S6 transmembrane domains, which is homologous to the P region of K channels (Heginbotham et al., 1992; Goulding et al., 1993).

Despite the progress in elucidating domains involved in CNG channel function, fundamental questions remain as to how many pore-forming subunits are present in the functional channel. Based on the sequence homology between CNG and voltage-gated K channels, the CNG channels may be tetramers. However, high resolution electron microscopy of purified and reconstituted complexes of the 63 kDa pore-forming subunits of retinal CNG channels suggests that the channels exhibit 5-fold symmetry (Eismann et al., 1993). Since the channels functionally resemble the pentameric ligand-gated channels, and exhibit Hill coefficients that are above 3 (Yau and Baylor, 1989), the channels may indeed be pentamers. This latter possibility could explain why the pore diameter of the cation nonselective CNG channels (around 6 Å; Goulding et al., 1993) is so much larger than the pore of the highly selective K channels (around 3–4 Å, Hille, 1973).

In this study, we have examined the subunit stoichiometry of CNG channels by coexpressing the wild-type retinal CNG channel α subunit (RET) with a chimeric subunit (RO133) that has a larger single channel conductance. By analyzing the conductance levels in the coexpression studies, and by constructing dimers of wild-type and mutant subunits, we conclude that the CNG channels are, in fact, tetramers. Moreover, we demonstrate that channels with identical subunit composition but different subunit order display distinct properties. This suggests that the control of subunit order may provide a further mechanism for generating diversity of channel function.

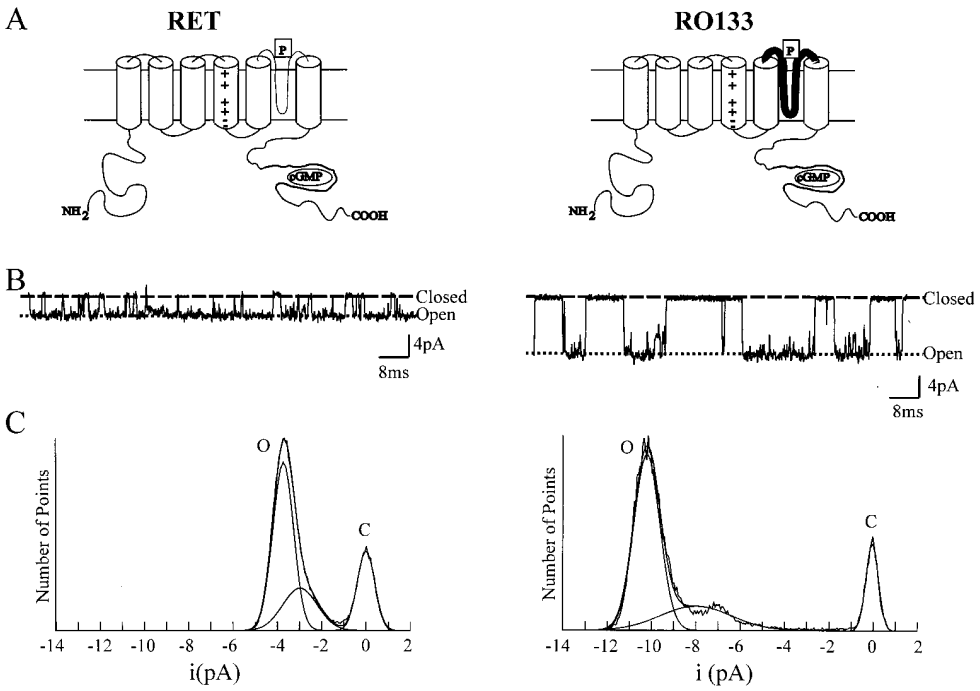

Figure 1. Properties of Homomultimeric RET and RO133 Single Channel Currents at Extracellular pH 9.0

(A) Cartoon of the bovine retinal channel (RET) and a chimeric channel (RO133). RO133 is a retinal channel with the RET P region replaced by the corresponding region from the catfish olfactory channel (bold line).

(B) Representative single channel records from inside-out patches containing either a single RET or RO133 channel at −120mV, extracellular pH 9.0 with Na^+ as the permeant ion.

(C) All points amplitude histograms for the RET and RO133 channels shown in (B). The histograms are fitted by three Gaussian functions. The peak labeled 'C' defines the fully closed conductance state. The peak labeled 'O' corresponds to the main open conductance state. A third Gaussian is required to fit an infrequently occupied subconductance state.

Results

Our approach to studying subunit stoichiometry is based on single channel conductance. We have previously shown that homomultimeric channels formed from the bovine retinal CNG channel α subunit (RET) have a smaller single channel conductance than channels formed from the homomultimeric catfish olfactory CNG channel α subunit (OLF; Goulding et al., 1993). We also showed that a chimeric retinal channel that contains the P region of the olfactory channel (RO133) displays a large conductance, similar to that of the olfactory channel, but retains RET-like gating by cyclic nucleotides. Furthermore, these differences in single channel conductance were shown to be due to differences in pore diameter, with the RET channel having a slightly narrower pore (~5.9Å) than that of OLF (~6.3Å) or RO133 (~6.4–6.5Å). We have here exploited these differences in single channel conductance by using the intermediate conductance of heteromultimeric channels formed from RET and RO133 subunits as a fingerprint of subunit stoichiometry.

One complication in using single channel conductance to characterize subunit composition is the presence of subconductance states that result from proton binding to the channel (Goulding et al., 1992; Root and MacKinnon, 1994). To facilitate detection of intermediate conductance channels that originate from heteromultimer formation, we have largely reduced (but not eliminated) the occupancy of the proton-induced subconductance states by using an extracellular solution wherein Na was the only permeant ion and the pH was raised to 9 (Root and MacKinnon, 1994). Under these conditions, there is a large difference between the main conductance state of RET (30 pS) and RO133 (85 pS; Figure 1).

Coinjection of RET and RO133 RNA into oocytes leads to the expression of channels with a number of distinct intermediate conductances. Figure 2 presents recordings from several patches containing multiple channels that demonstrate the presence of channels with conductances that clearly lie between those of homomultimeric RET and homomultimeric RO133 channels. Since channels with intermediate main conductance states were never observed in oocytes injected with either RET or RO133 alone, these channels are likely to arise from the formation of heteromultimers. Assuming that channel conductance is a function of the number of RET or RO133 subunits that form the channel, it should be possible to determine subunit stoichiometry simply by counting the number of distinct classes of intermediate conductance channels that are observed upon coexpression of RET and RO133. If only subunit composition matters and if CNG channels are tetramers, one would expect to see three intermediate conductance classes of channels (see Figure 4A). However, if CNG channels are pentamers, one would predict four intermediate conductance classes (Figure 4B).

To count the number of intermediate conductance classes, we obtained a large number of patches containing only a single channel, from oocytes coinjected with RET and RO133 RNA. Figures 3A–3F show sample

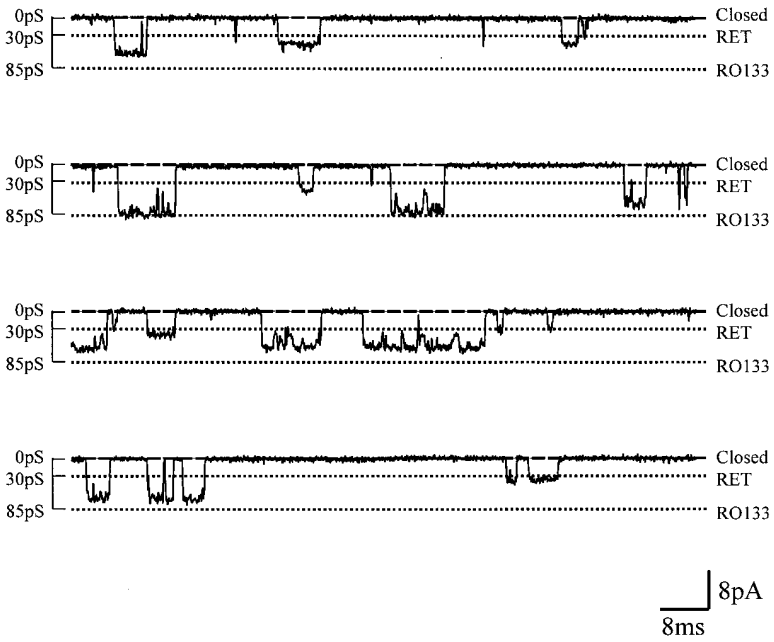

Figure 2. Intermediate Conductance Channels following Coexpression of RET and RO133 Indicate Heteromultimer Formation

Sample traces from multiple channel inside-out patches at −120mV in a low concentration of cyclic GMP (10–30 μM). Channels with conductances intermediate to RET and RO133 are present. The dotted lines indicate the zero current level (Closed) and the open channel current levels of homomultimeric RET and RO133, as indicated.

traces and all-points amplitude histograms from representative patches demonstrating the range of the different channel conductances observed. In each case, amplitude histograms were fitted by the sum of two or three Gaussian functions, with the two main Gaussian functions corresponding to the closed state (at 0 pA) and to the main conductance state of the unprotonated channel. In some patches, a third minor Gaussian was used to fit the subconductance state caused by residual protonation of the channel. Importantly, in all single channel patches, the main unprotonated channel conductance state was stable throughout the recording. That is, none of the channels were observed to undergo long-lasting transitions between more than one main conductance state. Therefore, the different main channel conductances seen in different patches must indicate the presence of channels with distinct subunit composition.

The data from all of our single channel recordings obtained from oocytes coinjected with RET and RO133 RNA were combined into a cumulative histogram, which plots the fraction of channels with conductances less than or equal to a given conductance level (Figure 4D). The histogram displays five distinct clusters of conductance values. The two extreme clusters of points correspond to homomultimeric RET (30 pS) and homomultimeric RO133 (85 pS) channels. The three intermediate clusters correspond to three major intermediate conductance classes of around 40 pS (level 1), 60 pS (level 2), and 73 pS (level 3). Thus, these data are consistent with the channel being a tetramer.

However, closer inspection of the points clustered at 40 pS reveals that these events are likely to reflect the contributions of two conductance classes of channels, one around 42 pS and one around 37 pS. Since the difference in conductance between the two channel classes is small, minor variations in conductance between experiments (e.g., due to small temperature or pH differences) obscure the separation between the conductances of the two populations. However, three lines of evidence suggest that there are indeed two distinct channel types present. First, the all-points amplitude histograms for individual 37 pS channels (Figure 3B) and 42 pS channels (Figure 3C) have a characteristically different shape, with the smaller conductance channel class spending a greater fraction of time in a subconductance state that requires a third Gaussian component. Second, the points clustered around 40 pS appear to fall into two separate peaks in a noncumulative histogram plot (Figure 5A). Third, some multi-channel patches contain both 37 pS and 42 pS channels, allowing a clear separation between the two channel types that is not obscured by small inter-patch variability (Figure 5B).

The presence of distinct 37 pS and 42 pS channel types indicates the existence of four intermediate channel conductances, consistent with the CNG channels being pentamers. However, another possibility is that the CNG channels are, in fact, tetramers and that the order of subunits around the central pore affects channel conductance. Thus, if CNG channels are composed of four pore-forming subunits, then channels with two RET and two RO133 subunits can be formed either with like subunits across from each other or with like subunits adjacent to each other. If the two arrangements of subunits result in channels that exhibit distinct conductances, a tetrameric channel would indeed yield four separate intermediate conductances in these mixing experiments.

Order of Subunits Affects Single Channel Conductance

Owing to the above ambiguity upon coexpression of RET and RO133 monomers, we next turned to dimer constructs, which allowed us to address the question of whether the order of subunits can affect channel conductance. Dimeric RET (RET-RET) and dimeric RO133 (RO133-RO133) channels, when expressed

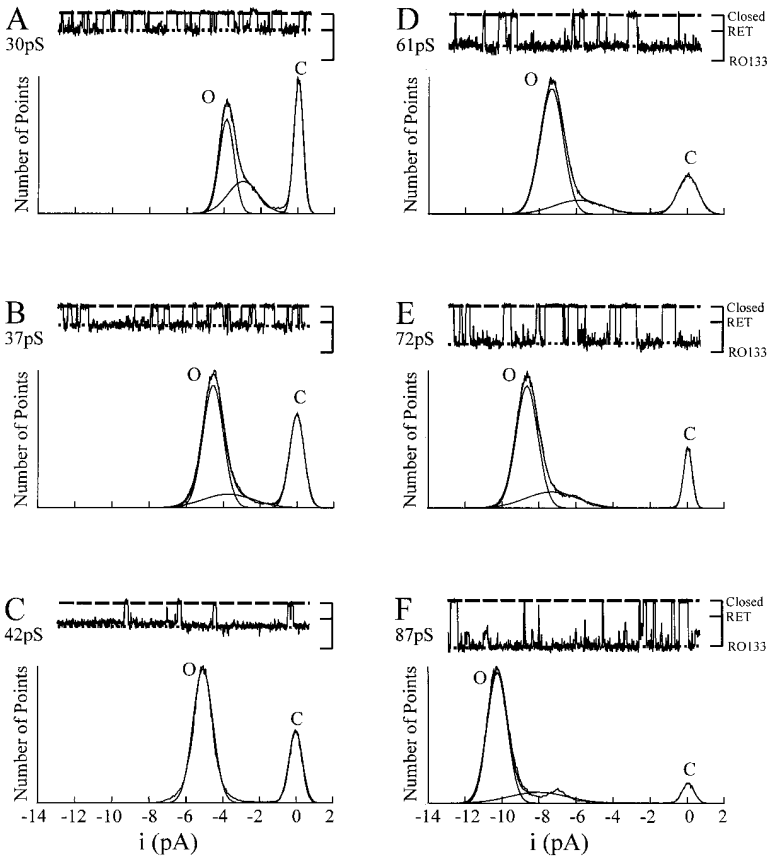

Figure 3. Sample Traces and All-Points Amplitude Histograms of Single Intermediate Conductance Class Channels

(A–F) All points amplitude histograms and representative stretches of data from 6 separate single channel patches illustrating the range of conductances observed. The histograms are fitted by two or three Gaussian distributions. Labels as in Figure 2. The conductance of each channel at −120mV is indicated. The channels in (A) and (F) have conductances similar to homomultimeric RET and RO133, respectively.

alone, yield functional channels with the expected single channel conductance of RET and RO133 homomultimers, respectively (data not shown). If CNG channels were tetramers, then coexpression of the two dimers should yield channels composed of either four RET subunits (channels with two RET dimers), four RO133 subunits (channels with two RO133 dimers), or two RET and two RO133 subunits (channels with one RET dimer and one RO133 dimer). Since in the latter case the order of subunits is likely to be fixed, with like subunits lying next to each other, only one intermediate conductance class should be observed (Figure 6A). In contrast, if CNG channels were pentamers, then coexpression of the RET and RO133 dimers would be expected to result in heteromultimers that include all four possible intermediate conductance channels expected for a pentamer upon coexpression of monomers (see Figure 6B).

Upon coexpression of RET and RO133 dimers, we obtained a total of 14 patches with intermediate conductance channels distinct from RET or RO133 homomultimers. As shown in Figure 6D, out of these 14 channels, 13 had identical single channel conductances of around 60 pS, corresponding to the intermediate conductance level 2 in the mixed monomer expression studies (Figure 4C). One channel had a conductance of 42 pS, corresponding to intermediate conductance level 1b. This pattern is very different from the monomer expression studies, where we observed significant numbers of channels in all four intermediate conductance levels. These results clearly favor the idea that CNG channels are tetramers, and that the 60 pS channel is formed by two RET and two RO133 subunits in which like subunits are adjacent to each other. The one channel with a conductance around 40pS could be due to minor monomer contamination of dimer DNA, RNA degradation, or incorporation of only one of the two subunits of one or more dimers into the channel.

The results with the dimers, although strongly suggestive that the channel is a tetramer, could be misleading if the RET and RO133 dimers did not freely coassemble (McCormack et al., 1992). For example, it is possible that the first subunit to be synthesized in each dimer may be favored or disadvantaged for inclusion into a channel. Furthermore, the data fail to elucidate the origin of the two closely spaced intermediate conductance levels of 37 and 42pS. Accordingly, we have constructed two heterodimers, RET-RO133 and RO133-RET, that differ in the order of the two subunits. If the channel is a tetramer and both subunits of a dimer contribute equally to forming the channel, then expression of either heterodimer alone should yield channels with only one, identical conductance (Figure 7A). Since the subunits in the two heterodimers are in a reversed order, a biased incorporation of the first or second subunit in a dimer would yield channels with different conductances. Expression of RET-RO133 heterodimers gave rise to channels with a conductance of around 40 pS in five out of six single channel recordings. All five channels recorded in single channel patches obtained from oocytes expressing RO133-RET dimers also had conductances around 40pS (Figure 7D).

The above results reinforce our conclusion that the channels are indeed tetramers, and that the two sub-

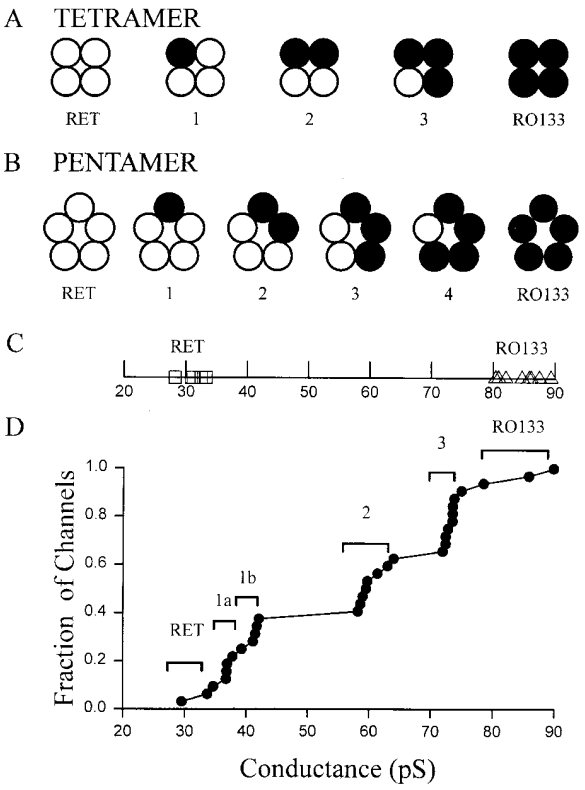

Figure 4. Clustering of Conductance Levels Is Consistent with Discrete Single Channel Conductances for Distinct Subunit Compositions

(A–B) Cartoons illustrating the possible heteromultimeric combinations of RET and RO133 subunits in tetrameric (A) and pentameric (B) channels. Closed circles represent RO133 subunits, while open circles represent RET subunits. Each combination could yield a heteromultimer with a distinct intermediate conductance level (numbered).

(C) One dimensional scatter plot of the conductances of six RET (open squares) and eight RO133 (open triangles) homomultimeric channels determined from single channel patches obtained from oocytes injected with either RET or RO133 cRNA alone.

(D) Cumulative histogram of channel conductances obtained from single channel patches from oocytes coinjected with RET and RO133 cRNA. The plot shows the fraction of channels with conductances less than or equal to a given conductance. Levels 1 (a and b), 2, and 3 indicate clusters of intermediate conductances around 40pS, 60pS, and 72pS, respectively. Of the 32 single channels recorded, three appear to be homomultimeric RET and cluster around 30pS, while three others cluster around 85pS and are likely to be homomultimeric RO133.

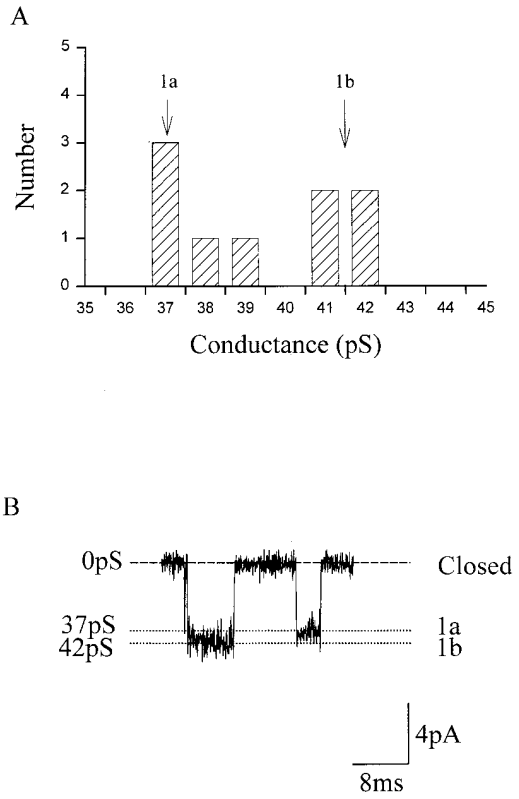

Figure 5. Possible Existence of Two Types of Channels within Level 1

(A) Noncumulative histogram of the channels with conductances near 40pS (data are replotted from Figure 4).

(B) Representative trace from a multiple channel patch that shows two well-resolved openings that have clearly distinct single channel currents around 37 and 42 pS.

units of the dimers are incorporated equally well. Moreover, these results reveal an intriguing difference in the single channel conductance between the heterodimers (40 pS) and the coexpressed homodimers (60 pS), despite the fact that in both cases, the functional channels presumably contain two RET and two RO133 subunits. One explanation for the difference in conductance is that the order of subunits is likely to be different between the two types of heteromultimeric channels. In heteromultimers formed between one RET dimer and one RO133 dimer, like subunits should lie next to each other. In channels expressed from the heterodimers, like subunits are likely to lie across the channel pore from each other (assuming that the dimers assemble tail to head, in which the carboxy terminal subunit of one dimer associates with the amino terminal subunit of the second dimer; see Figure 7A). Alternatively, a heterodimer may exist in a distinct conformation from a homodimer, leading to an allosteric change in channel conductance.

To distinguish between the above possibilities, we coexpressed RET-RO133 and RO133-RET heterodimers. This should yield two types of channels: those in which like subunits lie across from each other, and those in which like subunits lie adjacent to each other (formed from one RET-RO133 and one RO133-RET heterodimer; see Figure 7B). If subunit order was the reason for the difference between the 40 pS and 60 pS channels, we would predict that these experiments should yield a mixture of both conductances. If, on the other hand, an altered conformation of the heterodimers was responsible for the reduced conductance (relative to the 60 pS conductance channels), these mixing experiments should only yield 40 pS channels. As shown in Figure 7D, coexpression of the two heterodimers resulted in a weighted appearance of both 40pS and 60pS channels. Out of nine single channel patches, three channels had a conductance around 60pS, and six had a conductance around 40pS. Thus, the two heterodimers can indeed coassemble to form a larger conductance channel, suggesting that the difference between the 42 pS and 60

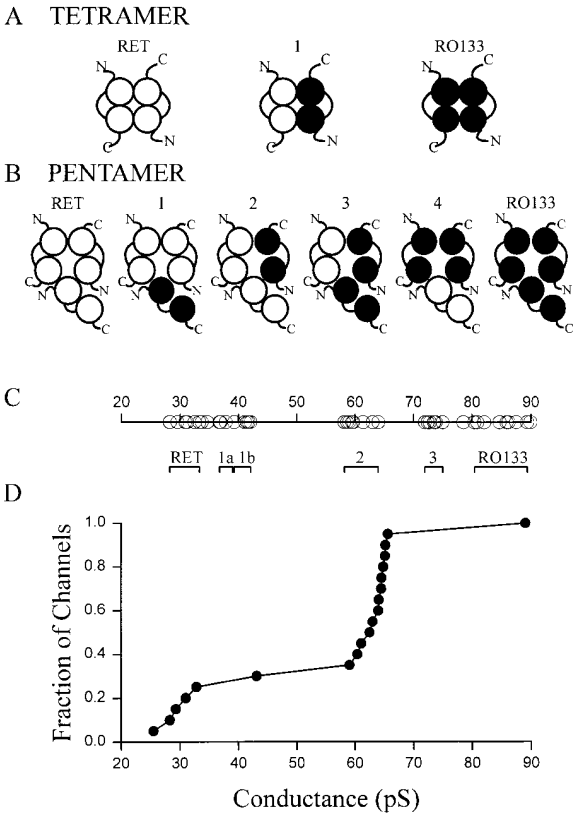

Figure 6. Coexpression of RET and RO133 Homodimers Constrains Subunit Assembly and Yields One Predominant Intermediate Conductance Class of Channels

(A–B) Potential subunit arrangements for tetrameric (A) and pentameric (B) channels formed by coassembly of RET dimers with RO133 dimers. Closed circles represent RO133 subunits, and open circles represent RET subunits.

(C) Monomer data from Figures 4C and 4D replotted as a one dimensional scatter plot for comparison. The range of each conductance level class identified from expression of RET and RO133 monomers are indicated.

(D) Cumulative histogram of single channel conductances from coexpression of RO133 and RET homodimers. The plot shows the fraction of channels with conductances less than or equal to a given conductance. The vast majority of intermediate conductance channels fall into a single conductance class around 60pS.

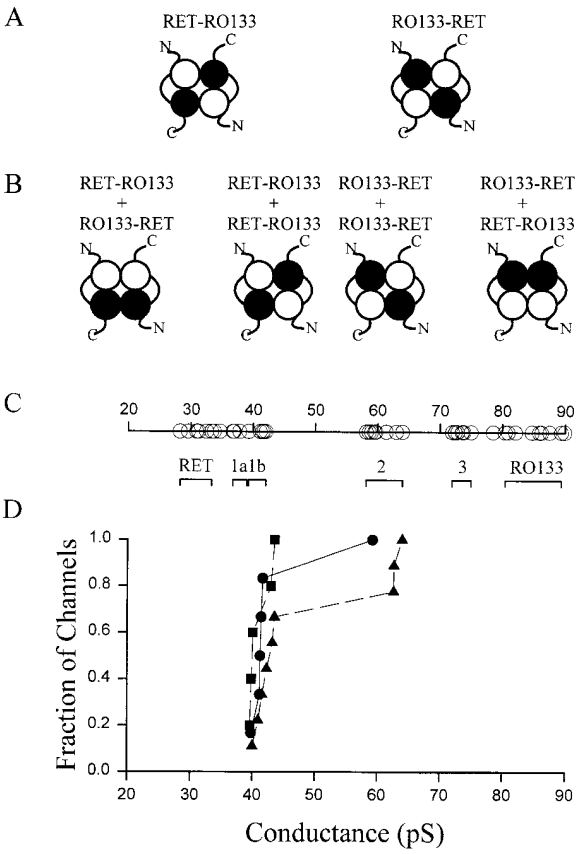

Figure 7. RET-RO133 and RO133-RET Heterodimers Reveal that Subunit Order Also Contributes to Determining Single Channel Conductance

(A–B) Channels formed by RET-RO133 or RO133-RET dimers expressed separately should be indistinguishable (A), while coexpression of these dimers should yield two separate families of channels (B).

(C) Monomer data from Figure 4C and 4D replotted as a one dimensional scatter plot for comparison. The range of each conductance level class identified from homomultimeric and heteromultimeric expression of RET and RO133 subunits are indicated.

(D) Cumulative histograms of conductances from single channel recordings from oocytes expressing either RO133-RET (closed squares) or RET-RO133 (closed circles) dimers alone and from oocytes coexpressing both RO133-RET and RET-RO133 dimers (closed triangles).

pS classes of channels reflects differences in subunit order. According to this interpretation, the 72 pS channel would be composed of three RO133 subunits and one RET subunit, whereas, the 37 pS channel would be composed of three RET subunits and one RO133 subunit. Consistent with this view, we find that the 72 pS channel is the predominant intermediate conductance class observed in recordings from oocytes injected with a high proportion of RO133 to RET RNA. Conversely, the 37 pS channel is the predominant intermediate conductance class seen in recordings from oocytes injected with a high proportion of RET to RO133 RNA.

Discussion

This study provides evidence that strongly suggests that a functional CNG channel is composed of four subunits, and therefore, is structurally similar to the 4-fold architecture of voltage-gated ion channels (MacKinnon, 1991; Catterall, 1992; Hofmann et al., 1994). Two homologous classes of CNG channel subunits have been identified (α and β or subunit 1 and subunit 2) (Chen et al., 1993; Liman and Buck, 1994; Körschen et al., 1995; Bradley et al., 1994). The α subunit, used exclusively in these studies, forms functional homomultimers when expressed in Xenopus oocytes or mammalian cell lines. These homomultimeric channels, however, differ from the native channels in photoreceptors and olfactory neurons in their single channel properties (see Zagotta and Siegelbaum, 1996). Although the β subunits do not form functional channels when expressed by themselves, when coexpressed with the α subunits, the resultant channels more closely resemble the native channels. Thus, it is likely that in native membranes the channels are heteromultimers, composed of homologous α and β subunits. Although our results do not indicate the

stoichiometry of α and β subunits in native channels, they suggest that both the number and the position of the different subunits may potentially contribute to defining the conductance phenotype of the channel. Recent results of Gordon and Zagotta (1995) demonstrate that the order of the subunits also affects channel gating. These authors demonstrated that the potentiation of rod CNG channels by Ni^{2+} occurs only when two subunits possessing a key histidine residue are adjacent to each other. This suggests that the Ni^{2+} binding site is formed by the interaction of histidine residues from two adjacent subunits.

Our results also raise the question as to how neighboring subunit identity can influence the conductance properties of a channel. One possibility is that the arrangement determines the strength of interactions between neighboring glutamate residues in the pore (E363) that form an external binding site for both protons and divalent cations (Root and MacKinnon, 1994). An alternative possibility is based on the geometry of the pore. In a previous study, we found that differences in conductance between the retinal and olfactory channels were correlated with differences in pore diameter, based on the permeability of different diameter organic cations (Goulding et al., 1993). The chimeric RO133 channel has both the larger single channel conductance of the olfactory channel, as well as the olfactory channel's wider pore, indicating the importance of the P region for determining channel size. The differences in pore diameter were shown to quantitatively account for the observed differences in channel conductance, based on a hydrodynamic theory for ion permeation (Dwyer et al., 1980). This latter result suggests both why subunit order affects conductance, and why the heteromultimers with like subunits across from each other have a single channel conductance that is close to that of RET homomultimers, despite the presence of the two large conductance RO133 subunits. Thus, if we model the RET subunits as having larger projections that constrict the pore, channels with two RET subunits across from each other will possess a pore whose diameter is considerably narrower than that of channels in which the two RET subunits are adjacent (Figure 8). Using the hydrodynamic theory, the predicted conductance for the two heteromultimers turns out to be 54pS and 30pS for the adjacent and opposed subunit arrangements, respectively (see Experimental Procedures). The difference of 24pS between the two is in good agreement with the observed difference of 18pS.

Thus, these results provide evidence that the cyclic nucleotide-gated channels are composed of four pore-forming subunits, strengthening their close relation with voltage-gated K channels. Moreover, we demonstrate that subunit order dramatically affects channel properties, in this case altering conductance values by 50%. Additionally, the fact that the heterodimers form channels in which like subunits are constrained to lie across from each other suggests that the channel subunits assemble head to tail with a 4-fold symmetry around a central axis. Finally, the ability to distinguish channel subunit composition and subunit order based on conductance properties provides a powerful approach for future studies of the mechanism and stoichiometry by which cyclic nucleotide binding leads to channel activation.

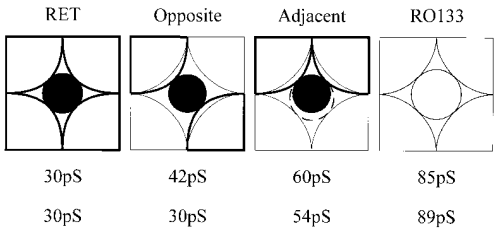

Figure 8. The Relationship between Subunit Order, Channel Pore Diameter, and Single Channel Conductance

Cartoon showing the largest circle that can fit into the pore of RET (closed circle) and RO133 homomultimers (open circle with solid outline), and 2RET:2RO133 heteromultimers with like subunits opposite (closed circle) or adjacent (dashed open circle) to each other. The bold outlined subunits represent RET, and the light outlined subunits represent RO133. Note that RET subunits extend further into the pore than RO133 subunits. The effective pore diameter of channels with like subunits next to each other (adjacent) is larger than the effective pore diameter of channels with like subunits lying diagonally across the pore (opposite). The effective diameter of a circle that can fit into the pore of a channel with like subunits opposite to each other is the same as the effective diameter of a RET homomultimer. The actual and predicted single channel conductances (from hydrodynamic theory of Dwyer et al., 1980) are also given.

Experimental Procedures

Molecular Biology

The bovine retinal CNG channel (RET) cDNA was subcloned in a modified vector pGEM-3Z (Promega) containing the 5′ and 3′ Xenopus β-globin untranslated sequences flanking the polylinker region (Goulding et al., 1993; Liman et al., 1992). The P chimera (RO133) was made using polymerase chain reaction (PCR) (Goulding et al., 1993). Briefly, two PCR products generated from a retinal channel template were isolated on gels and used as primers to generate a chimeric PCR product from an olfactory channel template. The chimeric PCR product was then subcloned into RET. RNA was transcribed from either NheI-linearized or HindIII-linearized DNA using T7 RNA polymerase and injected into Xenopus oocytes prepared as previously described (Goulding et al., 1992).

The dimer constructs were made using PCR and subcloning. A clone, RETSau-, which is RET with the SauI site abolished, was made using PCR site-directed mutagenesis. Then, using a 5′ primer with a linker ApaI site, a 3′ primer with a linker HindIII site, and BRET as the template, 0.8kb of the amino terminus of RET (including a functional SauI site) was amplified using PCR, and the fragment was gel isolated. The fragment was then digested with ApaI and HindIII, and subcloned into RETSau-, creating the clone, RETDV. Sequencing of the fragment amplified by PCR and flanking regions was done to verify the clone. RET-RET Dimer was made by digesting RET with SauI and HindIII, gel isolating the 1.6kb fragment, and subcloning the fragment into RETDV. RET-RET was verfied by the size of the linearized plasmid and restriction digest with SauI and HindIII. RET-RO133 was made by digesting RO133 with SauI and HindIII and then gel isolating and subcloning the fragment into RETDV. RO133DV was made by digestion of RO133 with BsmI, gel isolation of the 0.3kb fragment, and subcloning of the fragment into RETDV. RO133-RO133 and RO133-RET were made using methods analogous to methods used to make RET-RET and RET-RO133. The constructs were amplified in the SURE2 (Stratagene) bacteria cell line. Due to possible recombination events in the bacteria and monomer contamination, DNA was gel-purified twice post NheI linearization. RNA was transcribed as above, using the doubly purifed DNA. The DNA and RNA were run on gels to ensure that the DNA and RNA were of the correct size for dimers. In the dimer constructs, the last six amino acids of the first subunit (TDSTND) were replaced by amino acids ID.

The heteromultimeric channels formed from either monomers or dimers have a maximal open probability >0.85, similar to wild-type

RET homomultimers, suggesting that the channels are correctly assembled and function properly.

Electrophysiology

Single channel recordings were obtained from inside-out patches 1–6 days after RNA injection, using an Axopatch 200A integrating patch clamp amplifier (Axon Instruments, USA). The internal solution contained 97mM KCl, 10mM HEPES, 10mM EGTA, and 1mM EDTA (pH 7.2, KOH) for divalent cation-free recordings. The patch pipette solution contained 97mM NaCl, 10mM AMPSO, 10mM EGTA, and 1mM EDTA (pH 9.0, NaOH). The acquired data was stored on VHS tape via a VR10B Digital Data Recorder (Instrutech Corporation, USA) to a Sony-SLV400 VCR (Sony, Japan). Subsequently the data was low-pass filtered at 4 kHz and digitized at 20 kHz using a TL-1 DMA Interface (Axon Instruments, USA) connected to a 486–33 MHz PC. The single channel recordings were analyzed by the construction of all-points amplitude histograms in a program written in AXOBASIC (Axon Instruments, USA).

Modeling Using Hydrodynamic Theory

We assumed that the pore size is approximated by a circle whose diameter is equal to the narrowest distance between two opposing P regions. Given that the pore diameters of RET and RO133 are 5.9Å and 6.5Å, respectively, the diameter of the largest circle that can fit into the pore of a channel containing two RO133 and two RET subunits, with like subunits adjacent to each other, is 6.2Å (see Figure 8). In contrast, the diameter of the largest circle that can fit into the pore of a channel containing two RO133 and two RET subunits, with like subunits opposite each other, is 5.9Å (see Figure 8). The diameter of partially hydrated Na (4.5Å) is taken as the effective diameter of an oblate ellipsoid with rectangular dimensions of a Na ion in contact with one water molecule (4.7 Å $\times$ 4.1 Å). One can calculate the relative Na^+ conductances for pores of different diameter, using the following hydrodynamic equation (Dwyer et al., 1980): $P_{Na} = (1\text{-}a)^2\ (1\text{–}2.105a + 2.0865a^3 - 1.7068a^5 + 0.72603a^6)/(1\text{–}0.75857a^5)$, where a = q/d, q is the diameter of cation X and d is the pore diameter.

Acknowledgments

We thank Dr. William Zagotta for helpful advice with the dimeric constructs, and Huan Yao and John Riley for technical assistance.

The costs of publication of this article were defrayed in part by the payment of page charges. This article must therefore be hereby marked *"advertisement"* in accordance with 18 USC Section 1734 solely to indicate this fact.

Received February 5, 1996; revised April 2, 1996.

References

Bradley, J., Li, J., Davidson, N., Lester, H.A., and Zinn, K. (1994). Heteromeric olfactory cyclic nucleotide-gated channels: a subunit that confers increased sensitivity to cAMP. Proc. Natl. Acad. Sci. USA *91*, 8890–8894.

Catterall, W.A. (1992). Cellular and molecular biology of voltage-gated sodium channels. Physiol. Rev. *72*, S15-S48.

Chen, T.Y., Peng, Y.W., Dhallan, R.S., Ahamed, B., Reed, R.R., and Yau, K.W. (1993). A new subunit of the cyclic nucleotide-gated cation channel in retinal rods. Nature *362*, 764–767.

Christie, M.J., North, R.A., Osborne, P.B., Douglass, J., and Adelman, J.P. (1990). Heteropolymeric potassium channels expressed in Xenopus oocytes from cloned subunits. Neuron *4*, 405–411.

Cooper, E., Couturier, S., and Ballivet, M. (1991). Pentameric structure and subunit stoichiometry of a neuronal nicotinic acetylcholine receptor. Nature *350*, 235–238.

Dwyer, T.M., Adams, D.J., and Hille, B. (1980). The permeability of the endplate channel to organic cations in frog muscle. J. Gen. Physiol. *75*, 469–492.

Eismann, E., Bönigk, W., and Kaupp, U.B. (1993). Structural features of cyclic nucleotide-gated channels. Cell Physiol. Biochem. *3*, 332–351.

Gordon, S.E., and Zagotta, W.N. (1995). Subunit interactions in coordination of Ni^{2+} in cyclic nucleotide-gated channels. Proc. Natl. Acad. Sci. USA *92*, 10222–10226.

Goulding, E.H., Ngai, J., Kramer, R.H., Colicos, S., Axel, R., Siegelbaum, S.A., and Chess, A. (1992). Molecular cloning and single-channel properties of the cyclic nucleotide-gated channel from catfish olfactory neurons. Neuron *8*, 45–58.

Goulding, E.H., Tibbs, G.R., Liu, D., and Siegelbaum, S.A. (1993). Role of H5 domain in determining pore diameter and ion permeation through cyclic nucleotide-gated channels. Nature *364*, 61–64.

Heginbotham, L., Abramson, T., and MacKinnon (1992). A functional connection between the pores of distantly related ion channels as revealed by mutant K^+ channels. Science *258*, 1152–1155.

Hille, B. (1973). Potassium channels in myelinated nerve: selective permeability to small cations. J. Gen. Physiol. *61*, 669–686.

Hofmann, F., Biel, M., and Flockerzi, V. (1994). Molecular basis for Ca^{2+} channel diversity. Annu. Rev. Neurosci. *17*, 399–418.

Isacoff, E.Y., Jan, Y.N., and Jan, L.Y. (1990). Evidence for the formation of heteromultimeric potassium channels in Xenopus oocytes. Nature *345*, 530–534.

Isom L.L., De Jongh, K.S., and Catterall, W.A. (1994). Auxiliary subunits of voltage-gated ion channels. Neuron *12*, 1183–1194.

Jan, L.Y., and Jan, Y.N. (1990). A superfamily of ion channels. Nature *345*, 672.

Karlin, A. (1993). Structure of nicotinic acetylcholine receptors. Curr. Opin. Neurobiol. *3*, 299–309.

Körschen, H.G., Illing, M., Seifert, R., Sesti, F., Williams, A., Gotzes, S., Colville, C., Müller, F., Dosé, A., Godde, M., Molday, L., Kaupp, U.B., and Molday, R.S. (1995). A 240 kDa protein repesents the complete β subunit of the cyclic nucleotide-gated channel from rod photoreceptor. Neuron *15*, 627–636.

Liman, E.R., and Buck, L.B. (1994). A second subunit of the olfactory cyclic nucleotide-gated channel confers high sensitivity to cAMP. Neuron *13*, 611–621.

Liman, E.R., Tytgat J., and Hess, P. (1992). Subunit stoichiometry of a mammalian K^+ channel determined by construction of multimeric cDNAs. Neuron *9*, 861–871.

MacKinnon, R. (1991). Determination of the subunit stoichiometry of a voltage-activated potassium channel. Nature *350*, 232–235.

McCormack, K., Lin, L., Iverson, L.E., Tanouye, M.A., and Sigworth, F.J. (1992). Tandem linkage of *Shaker* K^+ channel subunits does not ensure the stoichiometry of expressed channels. Biophys. J. *63*, 1406–1411.

Mishina, M., Takai, T., Imoto, K., Noda, M., Takahashi, T., Numa, S., Methfessel, C., and Sakmann, B. (1986). Molecular distinction between fetal and adult forms of muscle acetylcholine receptor. Nature *321*, 406–411.

Nakamura, T., and Gold, G.H. (1987). A cyclic nucleotide-gated conductance in olfactory receptor cilia. Nature *325*, 442–444.

Root, M.J., and Mackinnon, R. (1994). Two identical noninteracting sites in an ion channel revealed by proton transfer. Science *265*, 1852–1856.

Ruppersberg, J.P., Schröter, K.H., Sakmann, B., Stocker, M., Sewing, S., and Pongs, O. (1990). Heteromultimeric channels formed by rat brain potassium-channel proteins. Nature *345*, 535–537.

Yau, K.W., and Baylor, D.A. (1989). Cyclic GMP-activated conductance of retinal photoreceptor cells. Annu. Rev. Neurosci. *12*, 289–327.

Zagotta, W.N., and Siegelbaum, S.A. (1996). Structure and function of cyclic nucleotide-gated channels. Annu. Rev. Neurosci. *19*, 235–263.